Journal of Sound and Vibration (1999) **227**(2), 397–407
Article No. jsvi.1999.2351, available online at http://www.idealibrary.com on IDEAL®

EXACT AND APPROXIMATE DIRECTIVITY PATTERNS OF THE SOUND RADIATED FROM A CYLINDRICAL DUCT

S. T. HOCTER

Department of Mathematics, University of Keele, Keele, Staffordshire, ST5 5BG U.K.

(*Received* 27 *January* 1999, *and in final form* 28 *April* 1999)

The exact solution for radiation from a cylindrical pipe obtained by using the Wiener–Hopf method has been available for over 50 years. Approximate solutions can be used to simplify the problem, and their accuracy compared with the exact solution. Firstly, the exact solution can be simplified by using the method of the steepest descent to cast the problem in the form of Weinstein's *U*-approximation. A simpler technique involves the use of the Kirchhoff approximation. This vastly simplifies the problem by considering the radiation emanating from a circular aperture in a thin screen. The various formulae are then compared in a parameter space related to the physical structure of a propagating model. If one considers the behaviour of the approximations solely as one of the governing parameters is altered (i.e., as k_0a is increased), the physical behaviour of the propagating mode would not linearly change. In considering the parameters in terms of mode angles, one can observe the accuracy of the approximations for various parameters while linearly changing the ray structure.

1. INTRODUCTION

The sound radiation from an unflanged cylindrical duct was calculated by the Wiener–Hopf technique some years ago by Levine and Schwinger [1] and Weinstein [2], and later workers who have used this technique include Homicz and Lordi [3] and Lansing [4]. The earlier work of Levine and Schwinger concentrated on non-spinning modes, which are modes with azimuthal order zero. Later work by Homicz and Lordi [3] includes directivity plots for spinning modes. The figures given by Homicz and Lordi illustrate the general structure of a directivity pattern with multiple lobes in the front half-plane that result from two rays interfering with each other, and show a broad lobe towards the rear of the duct. High azimuthal order and high-frequency calculations are of particular interest when considering the noise produced by turbofan engines, although these large parameters increase the computation necessary with the exact solution. When considering problems with large parameters, the next step is to either determine approximations to the exact solution using asymptotic methods or to consider simpler techniques that are valid in a high parameter limit.

A number of simpler techniques are available which can be used to give an approximation to the solution, two of which will be considered in this paper. The

0022-460X/99/420397 + 11 $30.00/0

first of these involves the use of Weinstein's U function. This is a complicated technique that requires some knowledge of the exact solution but produces an approximation valid for all θ. The U function has been extensively analyzed by Weinstein [2], primarily for plane-parallel waveguides and electromagnetic modes in circular waveguides. A ray-based approach to a parallel-plate duct has been used by Lee [5], with the exact solution also expressed in terms of the U function. It has also been noted that the U function can be related to multiply reflected rays, shown for the parallel-plate waveguide by Bowman *et al.* [6, see pp. 46, 47]. The classical work of Tyler and Sofrin [7] first identified the farfield modal directivity function, which is of a similar form to the Kirchhoff approximation used here. This approximation is a widely used technique which involves considering an acoustic source at the duct fact [7–10]. The nature of the approximation prevents the radiated field behind the plane of the duct rim from being determined. It is believed [11] that the Kirchhoff approximation is accurate only for angle near the principal lobe although results presented here show the usefulness of this approximation may have been underestimated for spinning modes.

It is convenient to introduce a modal ray structure to describe how the acoustic mode propagates through the duct so that the regions in which the approximations can be considered satisfactory and can be physically interpreted. Some aspects of the ray structure have been determined by earlier authors, with the importance of the "mode ray angle" noted [2, 9, 12]. To describe fully a propagating spinning mode, a further angle is required which is noted by Weinstein (problem 3.13 [2]) and used by Rice *et al.* [12]. This paper uses the analytic expressions for the mode angles determined by Chapman [11] which contains a detailed analysis of the ray structure of the radiated field, and is put to full use in reference [10] which notes that the mode ray angle corresponds to a "nil-shielding direction". The angles ϕ_{ms}, θ_{ms} and θ_m are used where ϕ_{ms} is the azimuthal mode angle, θ_{ms} is the polar mode angle, the mode ray angle of earlier references and θ_m is the "quiet-zone" angle.

This paper proceeds by describing the geometry of the problem and briefly stating the formulae used for calculation of the directivity patterns. A set of results are shown and analyzed for various choices of ϕ_{ms} and θ_{ms}, although any combination of the mode angles is possible. For example, another interesting choice would be to observe the results as $k_0 a$ is increased for a fixed cone, i.e., fixed θ_m.

2. ANALYSIS AND GEOMETRY

2.1. NOTATION

Consider an acoustic mode, denoted by A_{ms}, of the form,

$$p = p_0 \mathrm{e}^{-\mathrm{i}\omega t + \mathrm{i}m\phi + \mathrm{i}k_x x} \mathrm{J}_m(k_r r) \tag{1}$$

in a semi-infinite cylindrical duct of radius a, propagating towards the open end. A system of cylindrical co-ordinates (r, ϕ, x), shown in Figure 1, is used to describe the mode, with the duct aligned along the x-axis, lying in $x < 0$. In the above mode, p represents the pressure, t the time and the modal parameters are ω the frequency,

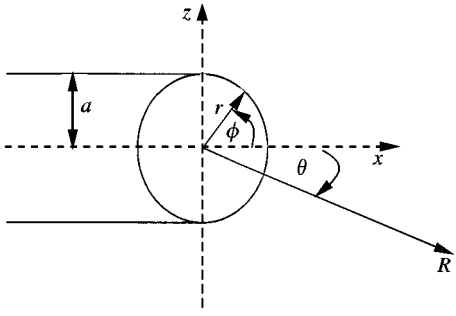

Figure 1. Cylindrical co-ordinates (r, ϕ, x) and spherical co-ordinates (R, θ).

m the azimuthal order, k_x the axial wavenumber and k_r the radial wavenumber. The duct wall at $r = a$ is assumed to be hard, so one can use the boundary condition $\partial p/\partial x = 0$ on $r = a$ which yields $J'_m(k_r a) = 0$. One can write $j'_{ms} = k_r a$ where j'_{ms} is the sth zero of J'_m, thus introducing the radial order s. The incident mode is also a solution of the problem, and when substituted into the wave equation leads to a second order differential equation based on the Bessel function $J_m(z)$, where Bessel's equation is satisfied provided that one has $k_x^2 = k_0^2 - k_r^2$, where $k_0 = \omega/c$ is the free-space wavenumber. The relationship between k_x and k_r is an important one; for fixed values of $k_0 a$ this determines which modes propagate (when k_x is real) and which modes evanesce. Note that $k_x \equiv k_x^{ms}$.

A number of angles can be introduced to describe the form of the propagating mode as it progresses along the duct. Define ϕ_{ms}, θ_{ms}, θ_m such that

$$\sin \phi_{ms} = \frac{m}{j'_{ms}}, \quad \sin \theta_{ms} = \frac{j'_{ms}}{k_0 a}, \quad \sin \theta_m = \frac{m}{k_0 a}. \tag{2}$$

These quantities are represented in Figure 2. The propagating ray forms a piecewise linear helix which can be considered as a continuation of a series of individual rays lying in planes tangent to some caustic cylindrical surface. At the duct wall, each tangent plane is "tilted" to the meridional plane at the angle ϕ_{ms}. Two tangent planes will intersect to give a straight line along the duct wall with a ray on one tangent plane joining a ray on the next to form a composite ray. Following a ray through successive tangent planes will give the helical ray structure shown in Figure 2(b) where each segment is at a polar angle θ_{ms} to the duct axis on the tangent plane. The propagating mode exits the duct at angle θ_{ms} to the duct axis so that θ_{ms} corresponds to the continuation of the incident ray along the cone of diffracted rays. In the farfield directivity plots, one can see that θ_{ms} is close to the location of the main beam.

When the ray strikes the rim of the duct, a Keller cone of diffracted rays forms, with the cone obtained by extending the incident ray from the duct and rotating the extended ray about the tangent to the rim [13, 14]. The cone is at an angle $\pi/2 - \theta_m$ to the tangent to the duct rim at the point of diffraction. With the vertex of the cone at every point of the rim, a family of cones is obtained which envelops two surfaces.

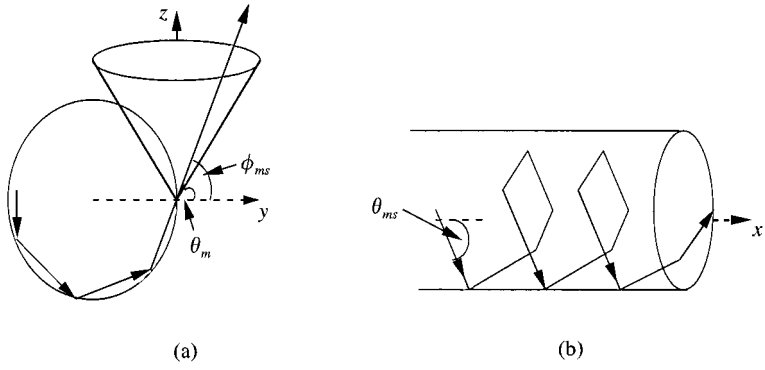

Figure 2. Ray geometry: (a) End view of the duct showing Keller cone at angle θ_m to y-axis and portion of propagating ray at angle ϕ_{ms} to y-axis, (b) side view of duct showing ray to be piecewise linear helix with each segment at an angle θ_{ms} to the duct axis.

In the far field, these tend to cones of angle θ_m centred on the forward and backward direction of the duct axis. No rays lie inside these cones, giving rise to the term "quiet-zone" angle for θ_m. An inspection of the directivity plots shows that the radiated field begins to decay rapidly in the forward and rearward directions at this angle. This phenomena is also clearly illustrated in the directivity plots of Homicz and Lordi (see Figure 2 of reference [3]).

An alternative method of viewing the ray is to project the piecewise linear helix into the meridional plane, so that the ray is composed of arcs of hyperbolae in this plane [11, 15]. The inset diagrams in Figure 3 show a segment of this projection, with the asymptotes to the meridional ray at an angle θ_{ms} to the duct axis. This pattern is repeated along the length of the duct after each reflection at the duct wall.

2.2. SUMMARY OF THE EXACT SOLUTION

To solve the problem with the Wiener–Hopf method, one considers a semi-infinite cylindrical duct lying axially along the x-axis for $x < 0$, with the duct rim lying in the plane $x = 0$. The kernel used in the Wiener–Hopf calculations is given by

$$K(k) = \pi\kappa a \mathrm{J}'_m(\kappa a)\mathrm{H}'_m(\kappa a), \quad \kappa(k) = \sqrt{k_0^2 - k^2}\,. \tag{3}$$

An exact solution is obtained that can be simplified in the far field by using spherical co-ordinates (R, θ, ϕ), and the power per unit solid angle derived such that

$$\mathscr{P}_{wh}(\theta) = \frac{P_i k_0 k_x^s}{\pi^2 (k_0 \cos\theta - k_x^s)^2} \frac{\mathrm{J}'_m(k_0 a \sin\theta)}{|\mathrm{H}'_m(k_0 a \sin\theta)|} \prod_{\substack{n=1 \\ \neq s}}^{N} \frac{k_x^n + k_x^s}{k_x^n - k_x^s}$$

$$\times \prod_{n=1}^{N} \frac{k_x^n - k_0 \cos\theta}{k_x^n + k_0 \cos\theta} \, \mathrm{e}^{\Re[S(k_x^s a) - S(k_0 a \cos\theta)]}, \tag{4}$$

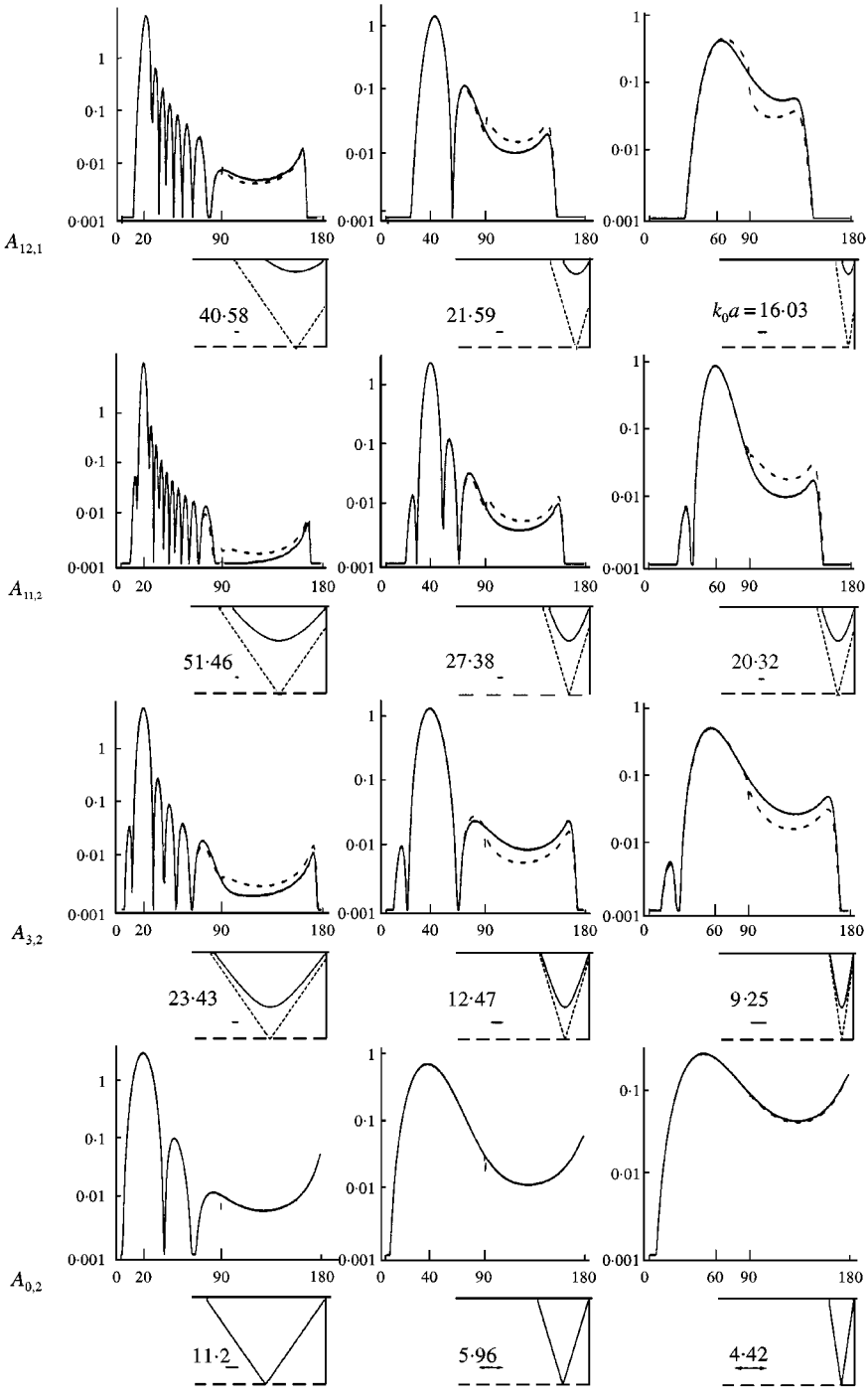

Figure 3. Radiated field directivity patterns showing exact solution (solid line) and *U*-approximation (dashed line) on a logarithmic scale, individually varying θ while varying ϕ_{ms} vertically and θ_{ms} horizontally. Overall, values of $\phi_{ms} = 0, 20, 40$ and 60° and $\theta_{ms} = 20, 40$ and 60° are used, with $P_i = 1$. The key for each pattern shows a segment of the three-dimensional incident ray projected into the meridional plane, the portion illustrated being from the duct rim back to the last reflection off the duct wall. The arrow denotes one wavelength λ such that $\lambda = 2\pi a/k_0 a$. The shorter dashed line represents the asymptotes of the meridional ray, which are at an angle θ_{ms} to the duct axis. The longer dashed line represents the centreline of the duct.

where N denotes the radial order of the highest propagating mode and P_i is the power of the incident mode. Energy conservation holds with the incident power being equal to the total radiated power plus the total reflected power. The reflected field has been determined for the exact solution and the U-approximation, showing that the reflected power is a very small proportion of the incident power for the spinning modes considered, although these results are outside the scope of this paper. Here, $\mathrm{H}_m(z)$ is the Hankel function $\mathrm{H}_m^{(1)}(z)$ with the superscript omitted. The function $\Re[S]$ is given by

$$\Re[S(\zeta)] = \frac{1}{\pi} P \int_{-k_0 a}^{k_0 a} \frac{\Omega(\kappa a)}{k - \zeta} \mathrm{d}k, \tag{5}$$

$$\Omega(k) = \tan^{-1} \frac{\mathrm{Y}'_m(k)}{\mathrm{J}'_m(k)} \pm \frac{\pi}{2}, \qquad \left\{ \begin{matrix} (+),\ m = 0 \\ (-),\ m \neq 0 \end{matrix} \right\}.$$

When using the Ω function it is necessary to include its phase, which is given by $\Omega(0) = 0$, $\Omega(j'_{ms}) = (s-1)\pi$ when $m \neq 0$. If $m = 0$, one must use $\Omega(j'_{ms}) = s\pi$. The integral above is taken in its Cauchy principal value sense, with all numerical integration performed by using NAG libraries.

2.3. APPROXIMATE FORMULAE

When using the Wiener–Hopf technique, it is necessary to factorize the kernel function into components that are analytic in two half-planes that overlap along a narrow strip. The decomposition of the kernal involves a complex integral which can be simplified by using the method of steepest descent. In approximating the kernel functions, one can reduce the integral to the canonical U-approximation that has been extensively analyzed by Weinstein [2], primarily for plane-parallel waveguides and electromagnetic modes in circular waveguides. For computational purposes, this is a simple function to determine with the numerical results produced significantly faster than the exact solution. The only drawback of this method is that it introduces a discontinuity at the sideline, which has the effect of "kicking out" the solution at the broad lobe in the rear half-plane. However, the size of this discontinuity decreases as $k_0 a$ is increased.

Using the method of the steepest descent to simplify the Wiener–Hopf kernel factors, denoted by $K_\pm(k)$, one obtains

$$K_+(k_0 \cos\theta) = \left\{ \begin{matrix} \mathrm{e}^{U(s_n, q)}, & \cos\theta < 0 \\ K(k_0 \cos\theta)\, \mathrm{e}^{U(s_n, q)}, & \cos\theta > 0 \end{matrix} \right\}, \tag{6}$$

where

$$U(s_n, q) = \frac{1}{2\pi i} \int_{-\infty}^{\infty} \ln(1 - \mathrm{e}^{2\pi i q - t^2/2}) \frac{\mathrm{d}t}{t - s_n \mathrm{e}^{\mathrm{i}\pi/4}}, \tag{7}$$

$$s_n = \sqrt{2k_0 a}\, \cos\theta, \quad q = \frac{1}{\pi} \Omega(k_0 a). \tag{8}$$

The power per unit solid angle of the radiated field is given by

$$\mathscr{P}_u(\theta) = \left\{ \begin{array}{cc} \dfrac{P_i k_0^3}{4\pi k_x^s (1 - m^2/j'^2_{ms})} & \dfrac{(k_x^s + k_0)}{(k_0 \cos\theta + k_0)} \dfrac{\sin^2\theta \mathrm{J}'^2_m (k_0 a \sin\theta) \mathrm{e}^{2\Re[U_s - U]}}{(k_0 \cos\theta - k_x^s)^2} \\ \dfrac{P_i k_0}{4\pi^3 k_x^s a^2 (1 - m^2/j'^2_{ms})} & \dfrac{(k_x^s + k_0)}{(k_0 \cos\theta + k_0)(k_0 \cos\theta - k_x^s)^2} \dfrac{\mathrm{e}^{2\Re[U_s - U]}}{|\mathrm{H}'_m(k_0 a \sin\theta)|^2} \end{array} \right\} \tag{9}$$

The first expression is for $\cos\theta > 0$, and the second is for $\cos\theta < 0$. In equation (9), $U \equiv U(s_n, q)$ and U_s is obtained by replacing θ with $\pi - \cos^{-1}(-k_x^s/k_0)$ in the expressions for U. The behaviour of the U-approximation is considered in greater detail in reference [2], Appendix B.

The second, and the most simple approximation considered involves the use of the Kirchhoff approximation. To determine the power of the radiated field using this method, one considers a circular aperture centred at the origin in a thin screen lying in the y–z plane. A scalar field, u_i, given by the propagating mode, is incident from the left ($x > 0$), and one takes $\partial u/\partial x = 0$ on the screen. The diffracted field is then taken as a double integral about the aperture by using the formula stated by Keller *et al.* [16]. This method accurately predicts the location of the principal lobe and the zeroes of the radiation pattern, as illustrated in Figure 4. An expression for the power per unit solid angle is given by

$$\mathscr{P}_k(\theta) = P_i \frac{k_0^3 k_x^s a^4}{\pi(1 - m^2/j'^2_{ms})} \left[\frac{\sin\theta \mathrm{J}'_m(k_0 a \sin\theta)}{(k_0 a)^2 \sin^2\theta - j'^2_{ms}} \right]^2. \tag{10}$$

3. ANALYSIS OF RESULTS

To determine suitable parameter spaces, one can consider the mode angles defined earlier so that one can relate the accuracy of the results to the physical structure of the ray within the duct. The relation $m < j'_{ms} < k_0 a$ which results from the properties of the Bessel functions, and the constraints upon propagating modes, place a constraint on the choice of angles possible. For example, one can only choose angles that satisfy $\sin\theta_m < \sin\phi_{ms}$.

The numerical results included in this paper show a comparison of the exact solution and the two approximations for ϕ_{ms} against θ_{ms}. A set of finite values for these two angles were chosen as stated in the caption of Figure 3. Results for $\phi_{ms} = 0^\circ$ are also included to illustrate the behaviour of the formulae if we consider a non-spinning ($m = 0$) mode. The results in this paper show a series of radiated field directivity patterns with a portion of the propagating ray projected into the meridional plane accompanying each graph. The directivity patterns use the spherical co-ordinates (R, θ, ϕ) introduced earlier, such that $\theta = 90^\circ$ is perpendicular to the duct axis, and $\theta > 90^\circ$ represents the field behind the duct opening.

The importance of the mode ray angle is clearly illustrated in the directivity patterns, although each of the formulae is singular at this point. An application of L'Hôpital's rule to equations (4), (9) and (10) shows that all three expressions agree

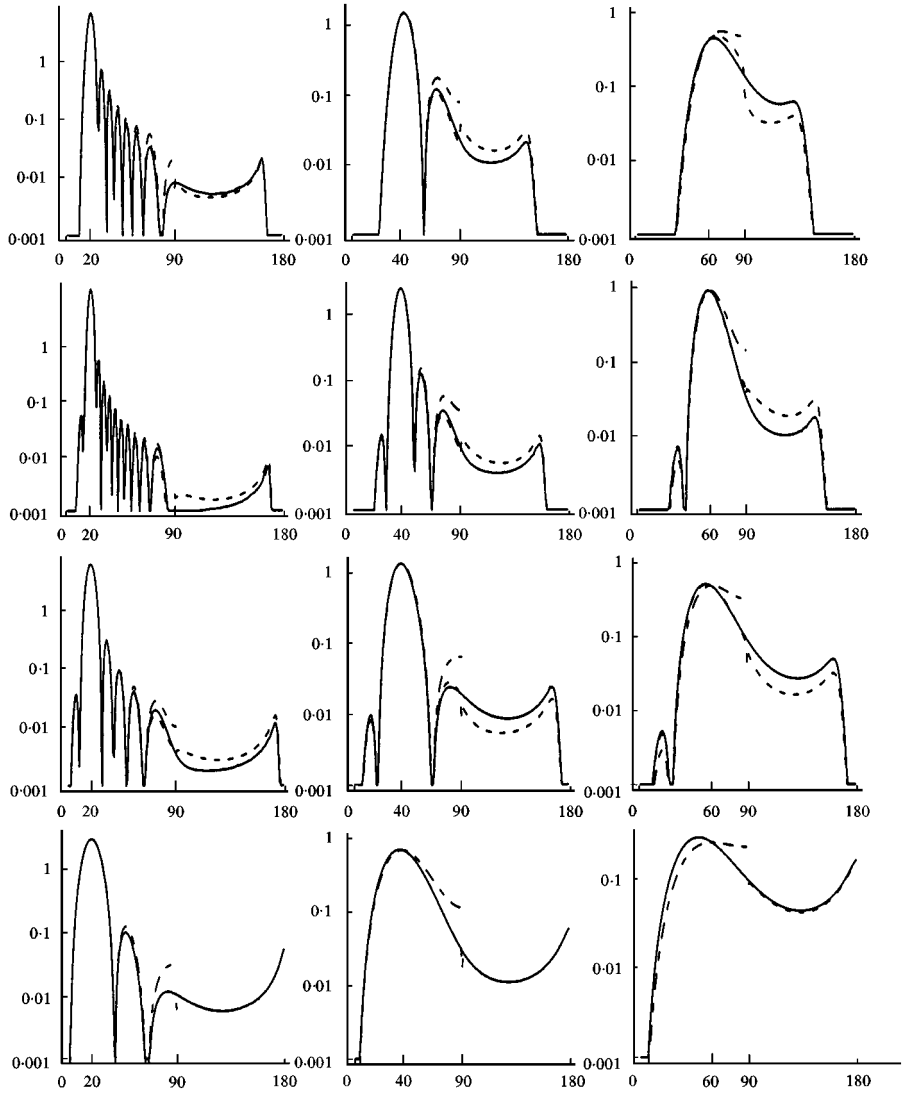

Figure 4. Radiated field directivity patterns showing exact solution (solid line), *U*-approximation (dashed line) and Kirchhoff approximation (dot–dashed line) on a logarithmic scale, individually varying θ while varying ϕ_{ms} vertically and θ_{ms} horizontally. Overall, values of $\phi_{ms} = 0$, 20, 40 and 60° and $\theta_{ms} = 20$, 40 and 60° are used, with $P_i = 1$. The meridional-plane ray structure and mode numbers are the same as that shown in Figure 3.

at this specific angle. The solutions rapidly tend to zero at either end of the plotted range so results were "chopped" below a certain point when graphed. We can see that this occurs at $\theta = \theta_m$, $\pi - \theta_m$ agreeing with statements made earlier, and in reference [11], that in the far field, no rays lie within cones of angle θ_m centred on the forward and backward directions of the duct axis. Furthermore, one wavelength λ is also denoted in this key. The number of lobes in the front half-plane decreases as we increase λ (equivalent to decreasing $k_0 a$). The second set of results show both approximations so that a comparison of all three expressions can be

made, though the meridional-plane ray figures have been omitted in this case since the ray structure is the same for both sets of results.

Although not explicitly shown, the formulae used here are appropriate for parameter regimes close to cut-off. However, if k_0a is small the U-approximation starts to breakdown, though it can be reformulated when $k_0a \approx j'_{ms}$ (problem 3.10 [2]).

3.1. THE U-APPROXIMATION

The nature of the U-approximation introduces a discontinuity at the sideline which can clearly be seen in Figure 3 having the effect of "kicking out" the solution as we pass this point. However, as noted by Weinstein [2], the size of the discontinuity decreases as one increases k_0a. Overall, it can be seen that decreasing the value of θ_{ms} results in the size of the discontinuity decreasing and improves the accuracy of the broad lobe in the rear halfplane. The U-approximation correctly predicts the minor lobes though it does show a slight degradation in performance near 90° which decreases for small θ_{ms}. Altering the value of ϕ_{ms} does not appear to have any effect on the accuracy of the results, although we are unable to obtain numerical results for large values of ϕ_{ms} because of the large values of m required in this region. The most surprising aspect of these results is the accuracy of the U approximation for the non-spinning mode case, where it is not possible to separate the two solutions except when θ_{ms} is large.

3.2. THE KIRCHHOFF APPROXIMATION

Results for the same parameter space as above showing how the Kirchhoff approximation performs in relation to the exact solution and the U-approximation are given in Figure 4. Only the approximation in the front half-plane is shown since the formula is symmetric about the sideline giving minor lobes behind the duct when one would only expect one broad lobe. The general degradation of the accuracy of this approximation near the sideline is clearly illustrated in this series of results. The formula accurately predicts the location of the zeroes, so when we decrease θ_{ms}, thus increasing the number of lobes, the overall accuracy of the approximation improves. When ϕ_{ms} is increased, the approximation degrades slightly with the solution at the minor lobes near the sideline being noticeably different from the exact solution. For the special case of non-spinning modes, the approximation degrades rapidly as we increase θ_{ms}, with the results only agreeing at θ_{ms} in the third curve.

4. CONCLUSIONS

This paper presents three formulae for the calculation of the sound radiated from a cylindrical duct in such a way that numerical solutions for any specific choice of governing parameters can be easily obtained. We consider two simplifications to

the problem ranging from a method that requires no knowledge of the exact solution to one with which it is necessary to perform some of the Wiener–Hopf manipulation. In this paper, we have only included results obtained when varying ϕ_{ms} with θ_{ms}, but further results have been produced for combinations involving θ_m and $k_0 a$.

Firstly, consider the behaviour of the Kirchhoff approximation which is simple to use, and does not require any extensive computation. The simplicity of this approach is reflected in the results being noticeably less accurate than the exact solution and failing completely in the rear half-plane. One also observes the approximation rapidly becoming inaccurate as the sideline is approached. The Kirchhoff formula accurately determines the location of the principal lobe, and all the zeroes, and is an ideal choice if only this information, or a rough outline to the general form of the radiation pattern is desired. It was expected that the Kirchhoff approximation would be accurate near the principal lobe and degrade for sideways radiation as seen in the $\phi_{ms} = 0^\circ$, $\theta_{ms} = 60^\circ$ case. Since this method is accurate at all the zeroes, as one changes the governing parameters such that the number of lobes in the front half-plane increases, the overall accuracy of the approximation improves increasing the range of accuracy much more than expected.

The *U*-approximation performs very well for much of the parameter space in the front half-plane where it is generally not discernible from the exact solution. The only drawback of this method is a slight discontinuity at the sideline which affects the broad lobe in the rear half-plane although this decreases as $k_0 a$ increases. As one changes the parameters to increase the number of lobes in the front half-plane, the accuracy of the approximation increases. The *U*-approximation is remarkably accurate for non-spinning modes with only the slight discontinuity at the sideline being evident. However, the exact solution is also much simpler to compute in this case.

In conclusion, the exact Wiener–Hopf solution for radiation from a cylindrical pipe is very complicated and numerically intensive. Two approximations have been introduced which can be used to simplify the solution, the first of which requires some knowledge of the exact solution whereas the second formula involves a simple use of the Kirchhoff approximation. These are just two of the possible approaches that can be used in producing a satisfactory approximation to the exact solution. Further work could consider the effect of other methodologies such as Keller's geometrical theory of diffraction using the three-dimensional ray structure described by Chapman [11].

ACKNOWLEDGMENTS

The author would like to thank Dr. C. J. Chapman for his advice throughout this work.

REFERENCES

1. H. Levine and J. Schwinger 1943 *Physical Review* **73**, 383–406. Radiation of sound from a circular pipe.

2. L. A. Weinstein 1969 *The Theory of Diffraction and the Factorization Method* (Generalized Wiener–Hopf Technique). Golem.
3. G. F. Homicz and J. A. Lordi 1975 *Journal of Sound and Vibration* **41**, 283–290. A note on the radiative directivity patterns of duct acoustic modes.
4. D. L. Lansing 1970 *Analytical Methods in Aircraft Aerodynamics* NASA SP-228, 323–334. Exact solution for radiation of sound from a semi-infinite circular duct with application to fan and compressor noise.
5. S. W. Lee 1972 *Journal of Mathematical Physics* **13**, 656–664. Ray theory of diffraction by open-ended waveguides. II. Applications.
6. J. J. Bowman, T. B. A. Senior and P. L. E. Uslenghi 1987 *Electromagnetic and Acoustic Scattering from Simple Shapes*. New York: Harper & Row.
7. J. M. Tyler and T. G. Sofrin 1962 *Society of Automotive Engineers Transactions* **70**, 309–332. Axial flow compressor noise studies.
8. C. L. Morfey 1969 *Journal of Sound and Vibration* **9**, 367–372. A note on the radiation efficiency of acoustic duct modes.
9. E. J. Rice 1978 *AIAA Journal* **16**, 906–911. Multimodal far-field radiation pattern using mode cutoff ratio.
10. C. J. Chapman 1996 *Journal of Fluid Mechanics* **313**, 367–380. Sound radiation from a cylindrical duct. Part 2. Source modelling, nil-shielding directions, and the open-to-ducted transfer function.
11. C. J. Chapman 1994 *Journal of Fluid Mechanics* **281**, 293–311. Sound radiation from a cylindrical duct. Part 1. Ray structure of the duct modes and of the external field.
12. E. J. Rice, M. F. Heidmann and T. G. Sofrin 1979 *Paper No. AIAA*-79-0183, *presented at the American Institute of Aeronautics and Astronautics* 17*th Aerospace Sciences Meeting*, *New Orleans*, *LA*, 15–17 January. Modal propagation angles in a cylindrical duct with flow and their relation to sound radiation.
13. J. B. Keller 1957 *Journal of Applied Physics* **28**, 426–444. Diffraction by an aperture I.
14. J. B. Keller 1962 *Journal of Optical Society of America* **52**, 116–130. Geometrical theory of diffraction.
15. A. M. Cargill 1989 *Internal Report TSG*0426, Rolls-Royce, Derby, England. Kirchhoff diffraction theory applied to a bell-mouthed duct.
16. J. B. Keller, R. M. Lewis and B. D. Seckler 1957 *Journal of Applied Physics* **28**, 570–579. Diffraction by an aperture II.